ORIGINAL PAPER

Effect of Face Losses and Cover-to-Diameter Ratio on Tunneling Induced Settlements in Soft Clay, Using Transparent Soil Models

Abdelaziz Ads · **Md Shariful Islam** · **Magued Iskander**

Abstract Reliable prediction of surface and subsurface settlements induced by shallow tunnels is important to minimize the adverse effects which may take place during tunnel excavation. A transparent soil surrogate representing the geotechnical behavior of soft clay was employed to explore spatial soil deformations within the soil mass near the tunnel. Shear strain, volumetric strain, surface and subsurface settlements resulting from increasing face losses were captured for three cover-to-diameter (C/D) ratios. The observed data trends are generally consistent with the data available in the literature, however the ability to visualize soil movements confirmed a number of perceived behaviors. First, the observed subsurface settlements are noticeably larger than surface ones. Second, the observed settlement trough widths are generally wider than the predicted ones, consistent with the low shear strength of the clay simulant. Third, calculated volumetric strains demonstrated the formation of an arching zone. Arching action slowly dissipates at higher C/D ratio, which may impact tunnel crown stability.

1 Introduction

Shallow tunnel construction, particularly in soft ground, has the potential to cause deleterious surface and sub-surface ground settlements that may damage existing buildings and sub-surface infrastructure. For this reason, the determination of ground settlement and strain fields in soil masses resulting from tunnel excavation is one of the most important topics in tunnelling research. Ground movement is a complex three-dimensional problem that is not only influenced by tunnel geometry and soil conditions, but also by construction details.

Observations of ground movement during tunneling operations have long been the primary source for understanding tunneling behavior in soft soils (Peck 1969; Clough and Schmidt 1981). These studies have been augmented by a variety of numerical studies to investigate surface and sub-surface settlements (e.g. Karakus and Fowell 2003). Nevertheless, experimental studies play a key role in quantifying ground deformations due to tunneling operations (Meguid et al. 2008). The ability to visualize sub-surface deformations is a recent important development in

A. Ads · M. Shariful Islam · M. Iskander (✉)
Department of Civil and Urban Engineering, New York University, Tandon School of Engineering, Six Metrotech Center, Brooklyn, NY 11201, USA
e-mail: iskander@nyu.edu

A. Ads
Structural Engineering Department, Tanta University, Tanta, Egypt

physical modelling of tunneling operations, which is employed in this study (Iskander 2010).

Cording (1975); Mair and Taylor (1997) summarized the main sources of settlements induced by shield tunneling to include: (i) Deformation of the ground towards the face resulting from stress relief or face losses. (ii) Radial ground movement during the passage of the shield. (iii) Radial ground movement into the tail void, due to existence of a gap between the tail of the shield and the lining. (iv) Deflection of the lining as the ground pressure increases, and (v) consolidation and/or creep processes in fine grained soils. Methods of calculating each component of ground loss have been reported by several authors including Cording et al. (1978), Attewell et al. (1986), Rowe and Lee (1992), among others. Dimmock and Mair (2007) identified four components of volume loss at the open-face St. James Park tunnel in clay, two components in front of the shield and two components behind the front of the shield. Movement towards the excavated face (*aka*. face loss) is one of the most important components of volume loss.

Tunnel face collapse mechanism varies in different soils. In sand, the tunnel face collapse often resembles a narrow chimney-shaped failure (Chambon and Corté 1994). The failure zone in clay is reported to be wider than sand extending outward and upward; usually wider than the tunnel diameter itself (Zhang et al. 2017). Failure typically initiates near the tunnel face and propagates toward the ground surface until a stabilizing arch is formed.

The effects of the overburden pressure ratio or cover-to-diameter ratio, *C/D* on face losses during tunnel excavation has received considerable attention, especially for shallow shield tunnels. Vu et al. (2016) summarized the effect of *C/D* on various components of ground loss. Several other studies explored the role of *C/D* in granular soils. Notably, Ahmed and Iskander (2011, 2012) visualized the zone of influence due to loss of face support using a transparent soil surrogate representing sand. The transparent soil modeling results were found to be in good agreement with the data reported by Dyer et al. (1996) in sand. Additionally, the observed zone of influence was similar to that obtained by Kirsch (2010) against an observation window in sand. However, the results were somewhat different from observations in clay.

Transparent soils have been employed to represent clay in many previous studies (e.g. Welker et al. 1999, 2000; Iskander et al. 2002; Liu and Iskander 2010; Ni et al. 2010). This study employs a different transparent soil surrogate to simulate the behavior of soft marine clay (Chini et al. 2015; Ads et al. 2020a). The work aims to estimate the magnitude of (1) surface and (2) sub-surface ground settlement and (3) visualize the extent of the affected zone for different face losses and cover-to-diameter scenarios. In addition, the resulting shear and volumetric strain in the supporting soils are also computed from the measured deformations. Results of these model tests will help practicing engineers to better identify the stages of collapse with increasing face loss. In this study, different face losses and cover to diameter ratios were examined to present the different stages of collapse from the beginning of soil movements till soil collapsing (*aka*, settlement exceeding the allowable limits). It will also provide a preliminary assessment during tunnel design about the risk to existing structures and sub-surface utilities in the affected area.

2 Prediction of Ground Settlement

The empirical Gaussian (normal distribution) curve shown in Fig. 1 was presented by Peck (1969) to predict the surface settlement trough above the tunnel. Peck's curve was adopted by many researchers such as Atkinson et al. (1975), Attewell (1978), O'Reilly and New (1982), and Cording (1991), among others. Although Peck's measurements were obtained behind the face at the tail of the shield, they remain popular for small scale experiments. For example, a series of the centrifuge tests presented by Schofield (1980) showed good agreement with the suggested Gaussian curve presented by Peck for surface settlement.

Loganathan and Poulos (1998), among others, developed closed-form solutions to predict tunneling induced ground movements. However, these are not commonly in use due to their relative complexity and current tunnelling practice relies largely on either numerical modelling (e.g. Kirsch 2010) or Peck (1969) Gaussian distribution curve shown in Fig. 1. This despite a variety of studies demonstrating deviation in field performance from the Gaussian curve (e.g. Marshall et al. 2012). The shape of the Gaussian settlement trough is described using the following equation:
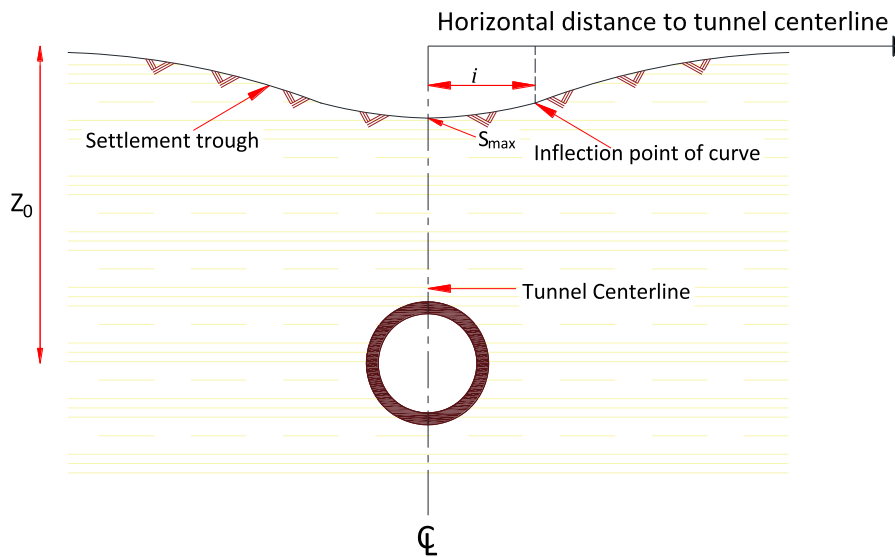
Fig. 1 Gaussian distribution curve representing tunnel settlement profile

$$S = S_{max}\exp\left(-\frac{x^2}{2i^2}\right) = \frac{V_s}{i\sqrt{2\pi}}\exp\left(-\frac{x^2}{2i^2}\right)$$
$$= \frac{AV_L}{i\sqrt{2\pi}}\exp\left(-\frac{x^2}{2i^2}\right) \tag{1}$$

where x is the distance from the centerline of a tunnel, i (or trough width) is the distance from the tunnel centerline to the inflection point of the trough, S_{max} is the maximum settlement, A is the tunnel cross-sectional area, V_s is the volume of the surface settlement trough per unit length of tunnel and V_L is the volume loss as a percentage of tunnel face volume per unit length of tunnel. The trough width (i) for surface and sub-surface settlement can be calculated by methods proposed by Mair et al. (1993) as follows:

$$i = K(z_0 - z) \tag{2}$$

The width of the settlement trough at a depth z depends on the depth of the tunnel z_0 (z = 0 at the surface) and the coefficient K depends on depth. The coefficient K can be calculated using the following equation:

$$K = \frac{0.175 + 0.325(1 - z/z_0)}{1 - z/z_0} \tag{3}$$

3 Experimental Investigation

The fundamental premise of this research is that transparent synthetic soil surrogates can be used to represent the behavior of natural soils in physical model tests (Hird and Stanier 2010; Ni et al. 2010; Ezzein and Bathurst 2011; Beemer and Aubeny 2012; Sun and Liu 2014; Chini et al. 2015; Iskander et al. 2015). This technique provides the ability to measure spatial deformation patterns within a soil mass. These deformations can then be used to infer strain fields within the measured continuum.

The experimental setup comprised of a 1-g physical model consisting of a horizontal tunnel, with a movable face. The tunnel was pre-placed in a clay surrogate, overlain by a constant thickness of sand, which acted as a surcharge. This investigation focused on the settlement inside the clay layer and at the clay/sand interface. The study explored the displacement in the clay to determine the influence of the overburden pressure ratio (C/D), also known as cover-to-diameter ratio, where C is the vertical distance from the top of the tunnel to the surface of the sand layer, and D is the tunnel diameter. Thus, overburden pressure consists of the totals stresses due to the weight of the clay plus the weight of the sand.

3.1 Transparent Clay and Its Properties

Magnesium Lithium Phyllosilicate (MLPS), commercially known as Laponite RD®, was chosen as the transparent soil surrogate, to represent soft clay. MLPS is similar to a natural hectorite clay. Geotechnical properties of MLPS were investigated by Wallace and Rutherford (2015) and concluded that the undrained shear strength, hydraulic conductivity, and compressibility parameters of MLPS are comparable to that of natural soft clay. The hydraulic conductivity of MLPS ranges between 5×10^{-9} cm/s to 1×10^{-7} cm/s which is consistent with that of many natural clays (Terzaghi et al. 1996). The permeability change index (C_k) for MPLS ranged from 0.5 to 0.87 of the initial voids ratio (e_0) which is in a good agreement with the reported values for soft clay ($0.5e_0$) and for Montmorillonite clay ($0.7e_0$) (Mesri and Ajlouni 2007). The coefficient of consolidation (c_v) varied depending on the percent of MLPS in the mix. c_v ranged between 0.008 and 0.050 m^2/year for MLPS from 4 to 15 % (Wallace and Rutherford 2015; Beemer et al. 2016). Dry MLPS particles are disk like being 25nm in diameter and 0.92nm thick. When hydrated the material absorbs approximately 200 times its weight and forms a colloidal structure whose geotechnical properties resemble that of soft clay (Ads et al. 2020b). Thus, the unit weight of MLPS after 28 days is 1.01 g/cm^3. In this study, 9 % MLPS was mixed with water and 0.45 % sodium pyrophosphate (SPP) to form a transparent slurry. The slurry was carefully transferred to the model chamber, paying attention not to introduce any air bubbles which are the primary source of transparency degradation. Samples were set aside for 10 days to age and gain strength. The shear strength of the models was determined by using a Miniature Ball Penetrometer and ranged between 0.8 and 1.6 kPa as shown in Fig. 2.

The undrained shear strength for soft soils typically increases with depth, due to the combined effects of consolidation, sedimentation, and increase in gravitational stresses. The ratio between the undrained shear strength to the effective stress which is known as C/P ratio for many soils is approximately 0.25 to 0.3 (Skempton 1957). The C/P ratio of the MLPS employed in this study was found to be 0.4 reflecting the high plasticity index of material reported by Wallace and Rutherford (2015).
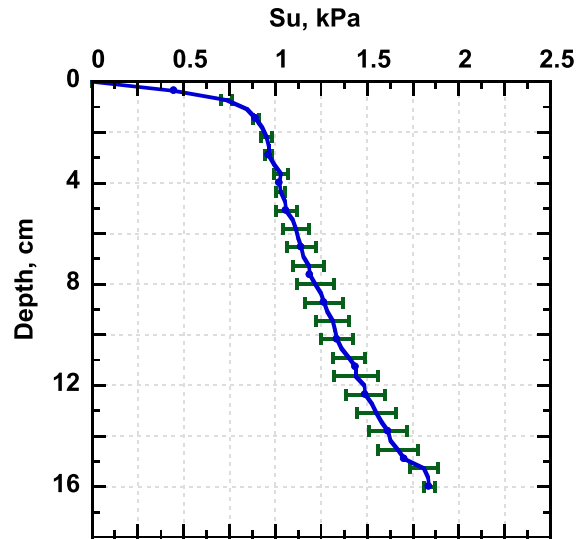

Fig. 2 Shear strength of the transparent soft clay simulant from ball penetrometer tests

3.2 Modelling of a Tunnel Excavation Using Transparent Clay

The tunnel model employed in this study is similar to the trap door model presented by Meguid et al. (2008). The method has been used by Davis et al. (1980), Adachi et al. (1997), and Mašín (2009), among others, to simulate tunnel face losses in clay. The hydraulic conductivity, permeability change index, compression coefficient, and the undrained shear strength of MLPS are comparable to that of soft clay (Wallace and Rutherford 2015). The reported hydraulic conductivity and consolidation properties suggest that the material is unable to drain during testing. Thus, MLPS surrogate and trap door method were used to simulate tunnel face collapse undrained soft clay soils. The model tunnel was made from a transparent acrylic rod, 57 mm in external diameter. The internal diameter of the tunnel was 50.8 mm, as shown in Fig. 3. A 6-mm thick plastic disk was used to simulate the tunnel face. The rear end of the tunnel face was attached to a threaded rod such that it did not come in contact with the soil in front of the tunnel face. A knob located at the end of this threaded rod, permitted retracting the tunnel face at a rate of 1.4 mm (3%D) per rotation. The tunnel face was manually retracted at a uniform rate of approximately 0.7%D/min (0.35 mm/min) and the maximum tunnel face movement was 18 mm or 35.4 % of the tunnel diameter. Three tests for three
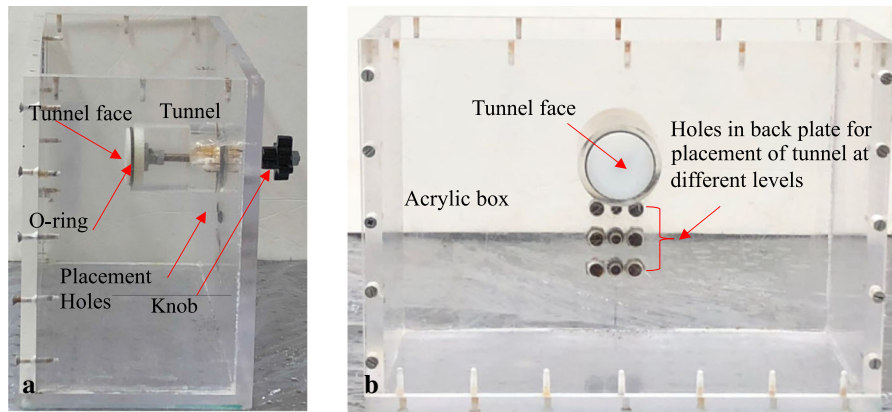
Fig. 3 Side (**a**) and front (**b**) view for the model and tunnel

cover-to-diameter ratios (1.5, 2.5, and 3.5) were conducted. Vertical displacements, horizontal displacements, and shear strains were determined from the analysis, for face losses ranging from 5%D to 30%D. Face loss is a different parameter and should not be confused with volume loss. Face loss represents the retracted face movement which correspond to the displacement of the tunnel crown as mentioned in Park and Adachi (2002) and Meguid et al. (2008), among others, whereas volume loss is the loss of ground around the tunnel face resulting a variety of tunnelling operations including from face losses.

The model chamber was made from 12.7 mm thick transparent acrylic sheet. The internal dimensions were 343 × 152 × 254 mm (L × W × H) as shown in Fig. 3. The dimensions of the chamber were chosen so that the distance from the tunnel center to the sides of the model chamber is at least 3 times the diameter of the tunnel, in order to minimize boundary effects. This ratio is consistent with the 2 to 4 diameters employed in several previous studies that succeeded in eliminating boundary effects (e.g. Atkinson and Potts 1977; Chambon and Corté 1994; Lee and Yoo 2006; Lee and Bassett 2007).

The model chamber was designed to be filled while it is lying on its side. The box has two removable sides, a front side and a top side, so that a layer of dyed particles could be inserted in the mid plane. The chamber has been filled in seven steps, according to a procedure detailed in Omidvar et al. (2016). First, the chamber was placed such that the tunnel was vertical, and its face pointing upwards, parallel to the chamber surface. Second, the chamber was filled with

transparent slurry to exceed the tunnel face level by 3 mm. Third, the sample was left for an hour to gain the required undrained shear strength to support an embedded plane composed of small dyed fused quartz particles that passed a #40 sieve and retained on a #60 sieve. Fourth, dyed fused quartz particles were sprinkled to create a monolayer thick embedded plane, particles were spread carefully to avoid any interaction with each other and the space between the particles was kept large enough to allow smooth movement of the particles with the MLPS. Later, the sample left for another hour to make sure the particles remain at the same position during the casting of the second half of the model. Fifth, the rest of the chamber was filled with the transparent slurry. Next, the box was rotated 90° so that the embedded plane became vertical. Finally, a 1D thick layer was removed from the top of the model and replaced by a layer of saturated Ottawa sand, to act as a surcharge load equal to 780 N/m^2. The same sand layer was employed in all tests, however the thickness of the soil beneath the tunnel varied depending on the C/D ratio.

3.3 Image Acquisition

Images were captured using a Nikon D3200 camera equipped with a Nikkor 2158 lens having a focal length of 18–55 mm and a maximum aperture of 1:3.5. The lens was focused on the embedded black particles, and its exposure was adjusted using the lens aperture, to achieve maximum contrast. The camera was adjusted to capture one frame each minute. Two 75-W LED lights placed behind the camera, were

employed to uniformly illuminate the model (Fig. 4). LED lights having a light color-temperature of 5600 K were selected to provide bright illumination. LED lights were selected to prevent increasing the model temperature, since the test duration is more than one hour. The refractive index of MLPS is somewhat temperature dependent, which may adversely impact transparency, if tungsten lights were used.

3.4 Measurement of Strain and Settlement Using Digital Image Correlation

In the past 20 years, Digital Image Correlation (DIC), also known as Particle Image Velocimetry (PIV) has increasingly become a common means for determining spatial deformations of soils (Arshad et al. 2014; Chen et al. 2015). DIC has been applied to investigate 2D deformations due to tunnel excavation in cohesionless soil (Ahmed and Iskander 2011, 2012; Idinger et al. 2011; Sun and Liu 2014). DIC employs a correlation function to locate the best matching position of two images, before and after deformation, to determine the average displacement between the two images.

A simple DIC technique has been proposed by Sadek et al. (2003) and Liu and Iskander (2004) to measure soil deformations inside transparent soils. The technique involves dividing the area of interest into a number of interrogation windows, and tracking successive movements within corresponding windows. The movement of each window represents the deformation of a specific area within the captured image. The analysis begins with larger windows, on the order of 5×5 mm that are split with every iteration of the analysis into smaller sub-windows that are shifted to track movements. The process continues until the entire deformation field is divided into sub

windows representing areas on the order of 2.5×2.5 mm. In this study, a similar approach was used to track movements of a speckle plane made by the embedded particles which were pre-placed within the model. DIC was carried out by using PIVview 3 C software. A zero-mean normalized sum of squared difference (ZNSSD) correlation function was used to track movements of corresponding windows. ZNSSD minimizes the sum of the difference between corresponding interrogation windows (Chen et al. 2016). The initial window size selected for this analysis was 96×96 pixels, and the final window size was 64×64 pixels, with an overlap of 50 %, which resulted in displacements calculated on a grid of 32×32 pixels, corresponding to 5 % of the tunnel diameter.

Vertical and horizontal displacements were obtained for each node directly by resolving the DIC displacements into their vertical and horizontal components. Nodal displacements and shape functions for each triangle were used to calculate the displacement matrix as suggested by Oñate (2013). An approach developed by Omidvar et al. (2015) was used to calculate shear and volumetric strain from the displacement matrix.

4 Results and Discussions

4.1 Shear Strain

Shear strains were calculated using nodal displacements obtained from DIC. Constant strain triangles (CST) were computed for three distinct *C/D* ratios at different face losses are shown in Fig. 5. The effect of shear strain extended vertically to the surface for C/D = 1.5 and 2.5, while for C/D = 3.5, the shear
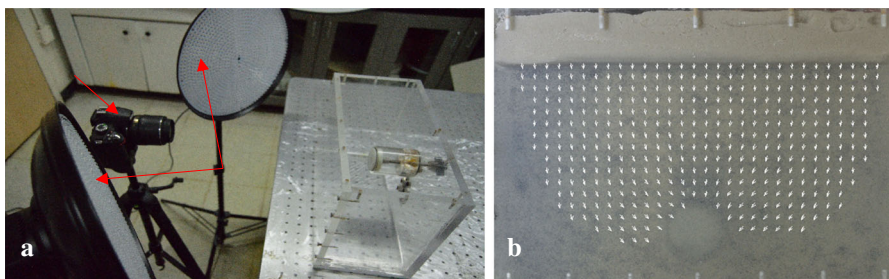
Fig. 4 Test setup (**a**) and front view (**b**) of the model showing transparent soil and seeded Plane
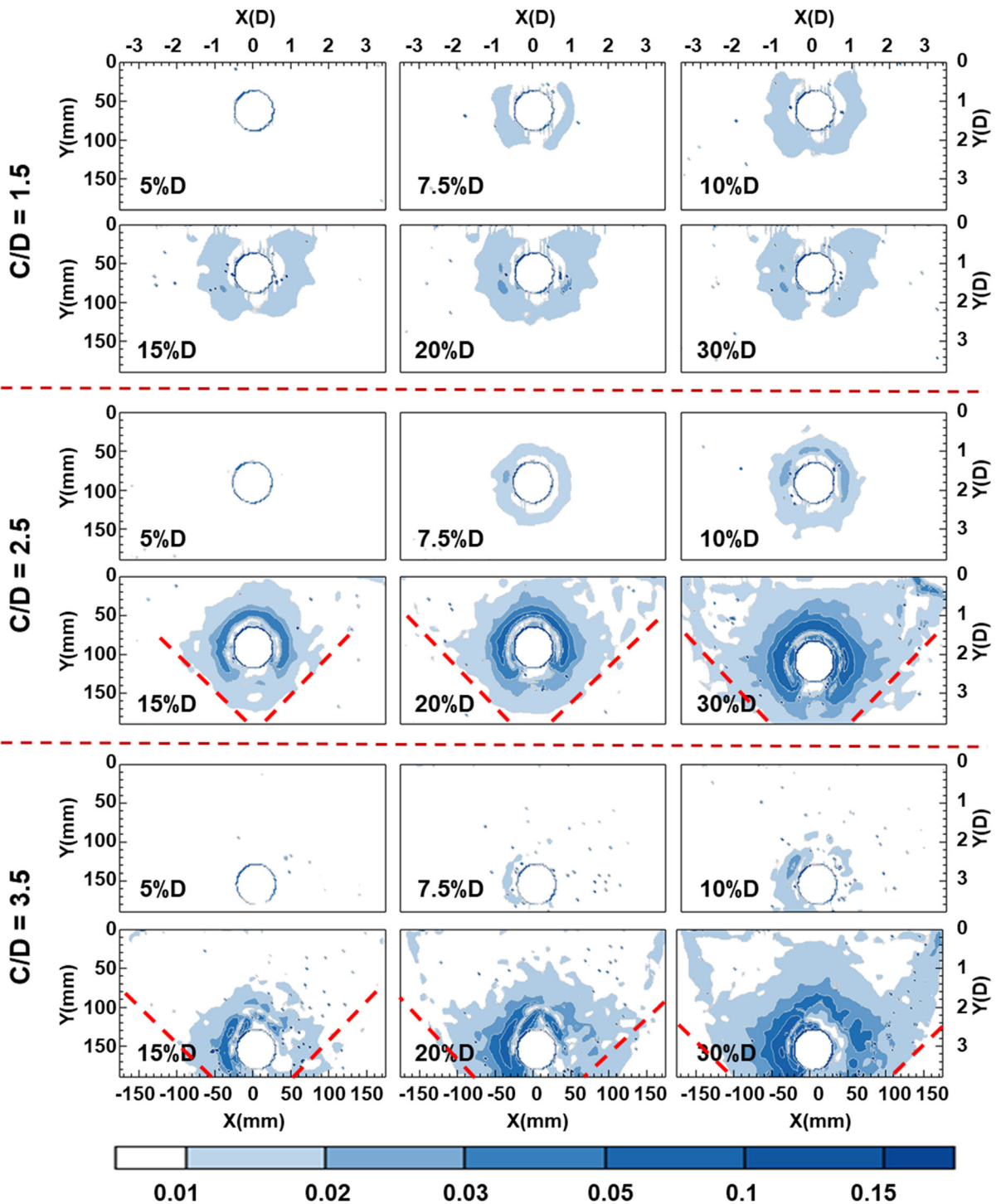
Fig. 5 Shear strain for cover-to-diameter ratio 1.5D, 2.5D, and 3.5D at different face losses (shear strain dimensionless)

strain zone extended up to 1.5D above the tunnel crown.

At face losses smaller than 10%D, the higher the *C/D* ratio, the smaller the shear strain zone. For

C/D = 1.5, shear strain values were 0.01–0.02 in a radius of 1.5D around the tunnel axis, and less than 0.01 in the remainder of the profile. With the increase in overburden pressure, the extent of shear strain decreases at face losses less than 10%D, extending only 1D from the tunnel axis. This is believed to have resulted from the increase in the shear strength of MLPS with depth. Conversely, as the face losses increases beyond 10%D, the extent and magnitude of shear strains increase at all *C/D* ratios. At these face losses the available shear strength was not able to sustain support. Shear strains increased with the increase in *C/D* ratios; at C/D = 2.5 and 3.5, the increase of the face losses from 15%D to 30%D, led to the shear strain zone rapidly widening up.

For face losses up to 5%D, no significant shear strain is observed at all *C/D* ratios. A distinct shear failure was not observed at C/D = 1.5 at any face losses. However, with the increase in the face losses, shear failure is observed when face loss exceeds 10%D for all *C/D* ratios larger than 1.5. This is consistent with centrifuge experiments in sand reported by Idinger et al. (2011). For C/D = 2.5 and 3.5, the failure zone widened up before the failure propagated to the surface forming a shear failure plane inclined by approximately 45° with the ground surface, the 45° lines are marked on Fig. 5 as dashed line.

4.2 Volumetric Strain

Volumetric strains at different overburden ratio are shown in Fig. 6. For C/D = 1.5, all the affected areas were subjected only to dilation regardless of the face losses and it was concentrated around the tunnel. The affected area around the tunnel grows as the face loss increases. The width of the dilative zone is less than 0.5D around the tunnel and the maximum volumetric strain within this area is equal to 0.3.

For C/D = 2.5, dilation is observed throughout the affected area until the face losses reach 10%D; after that, a compression zone forms an arch shielding the tunnel and the dilation zone from the overburden stress. The magnitude of the maximum compressive and dilative strains were 0.25 and 0.31, respectively, at 10%D face loss. Gnilsen (1989) reported both longitudinal and transverse arching developing to redistribute stresses around the tunnel face to stabilize it, and these observations are consistent with that.

For C/D = 3.5, the compression area starts at face loss 15%D but does not form a true arch. This behavior agrees well with Lee et al. (2006), who reported that shallower tunneling imposes a larger arching effect on the surrounding soil mass. The magnitude of the maximum compressive and dilative strains at C/D = 3.5 were 0.18 and 0.22, respectively, at 10%D face loss. Kong et al. (2018) also reported effect of cover depth on arching and presented that the arching action dissipates as the cover depth increases.

4.3 Surface and Subsurface Settlement

Vertical subsurface settlement for three *C/D* ratios at six different face losses are shown in Fig. 7. In general, subsurface settlements are noticeably larger than surface ones as previously reported in several studies (Moh et al. 1996; Park 2005; Ahmed and Iskander 2011, 2012). Trough widths at different face losses and C/D ratios were obtained from the vertical displacement based on DIC analysis shown in Fig. 7. Trough width decrease with the increase in *C/D* ratio. Settlement magnitude and trough width both increase with the increase in face losses. There are symmetric vertical subsurface movements under the tunnel invert level and the extent of these movements' decreases with the increase of the *C/D* ratio. These movements agree with observations presented by Mašín (2009). The trough width increases with the increase of the face loss until it reaches 15%D, after that there is no noticeable increase in trough width even though the value of subsurface settlement increases with *C/D*.

For C/D = 1.5, the maximum subsurface settlement occurred at a face loss of 15%D and after that subsurface settlement remained constant. For C/D = 2.5 and 3.5, the maximum subsurface settlement increased linearly from the beginning of face loss (5%D) to the end (30%D). The relationship between the maximum surface settlement and the face losses is shown in Fig. 8. It is evident that, the rate of change in surface settlement decreases with the increase of *C/D*. Park and Adachi (2002) and Thongprapha et al. (2015) observed similar behavior in their trapdoor model tests. But the trend is less clear for subsurface settlement, because subsurface settlement stabilizes after a face loss of 10–15 % of D. Maximum subsurface settlement due to change in cover-to-diameter ratio and face movement are also shown in Fig. 9. Again, subsurface settlements for C/D = 1.5
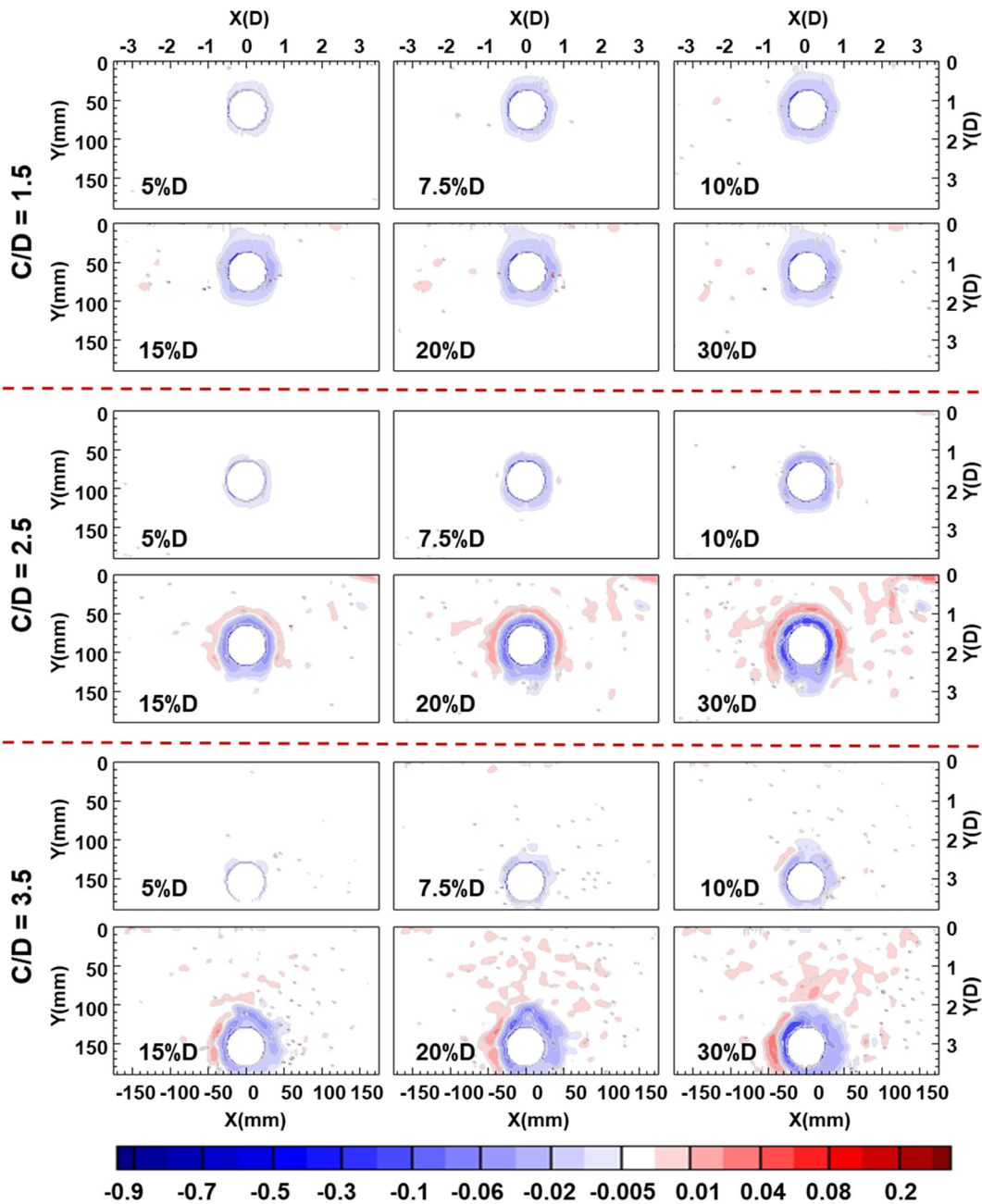
Fig. 6 Volumetric strain for cover-to-diameter ratio 1.5D, 2.5D, and 3.5D at different face losses (Blue for dilation is negative and red for compression is positive. Volumetric strain is dimensionless)

stabilize at a face loss of approximately 10%D, but not for C/D = 2.5 and 3.5. However, subsurface settlements of C/D = 2.5–3.5 are larger than C/D = 1.5 for all face losses, despite surface settlements being less for C/D = 2.5 and 3.5 than C/D = 1.5, for face losses up to 15–20%D (Fig. 7).

The relationship of observed volume loss (V_L) and face losses is explored next. First, the volume of the trough (V_s) was obtained using Eqs. (1)–(3) and the maximum settlements (S_{max}), assuming a Gaussian distribution. Next, Volume loss was computed as $V_L = 4V_s/\pi D^2$. The volume losses obtained are plotted
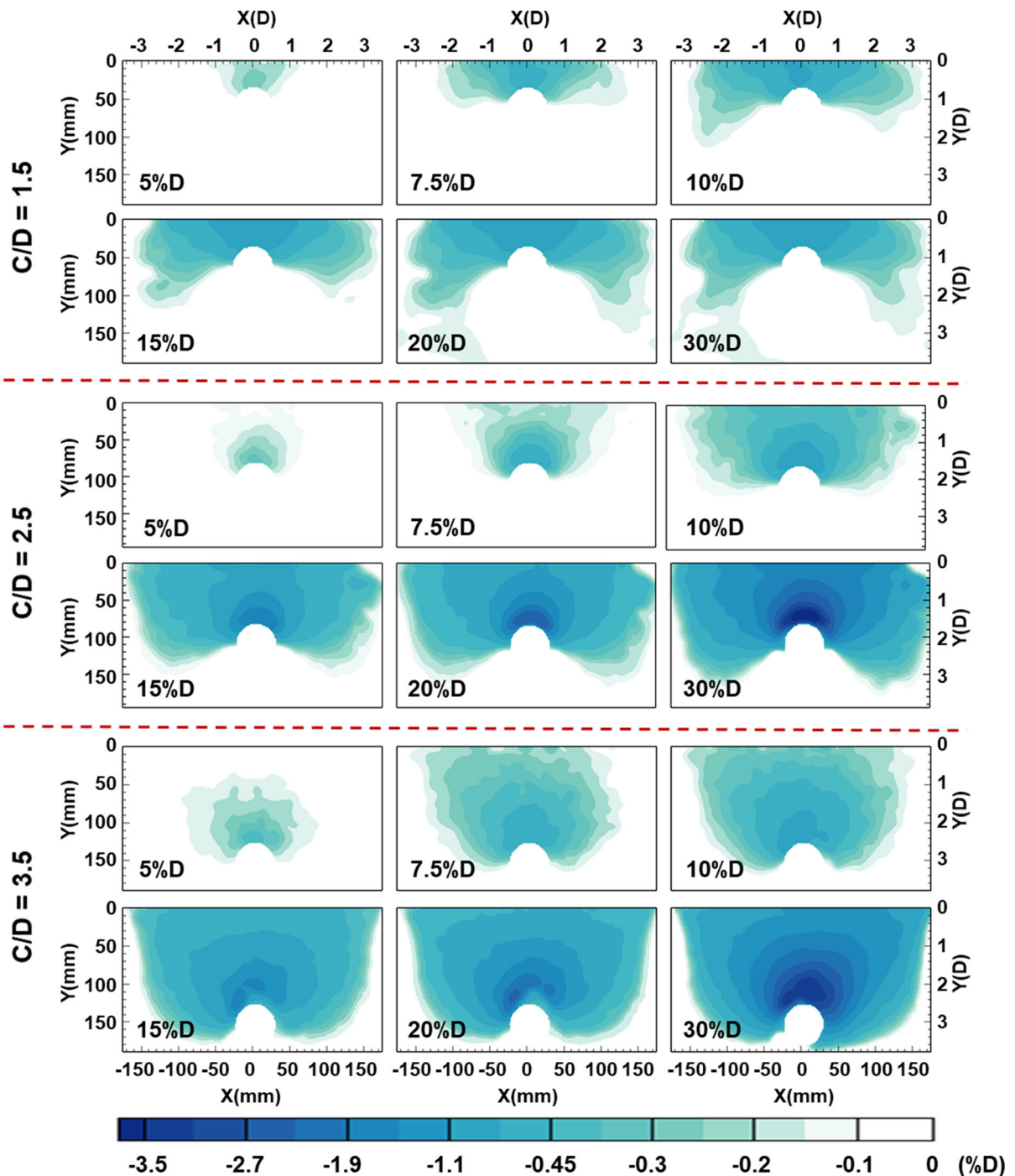
Fig. 7 Vertical settlement for cover-to-diameter ratio 1.5D, 2.5D, and 3.5D at different face losses

against face losses in Fig. 10. Volume loss increases with the increase of both *C/D* and face loss. The data suggests that face losses up to 10%D are typical of volume losses that may be experienced during

tunneling (up to 2 % volume loss), while larger face losses are representative of post failure behavior. The location of the embedded plane, a small distance away from the tunnel face may affect the relationship

Fig. 8 Maximum surface settlement due to change in cover-to-diameter ratio and face losses
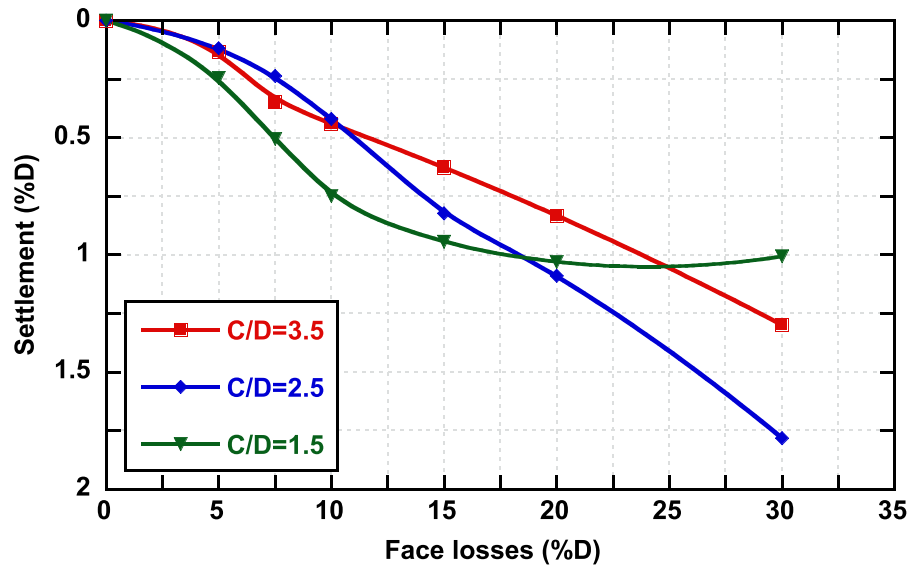
Fig. 9 Maximum subsurface settlement due to change in cover-to-diameter ratio and face losses
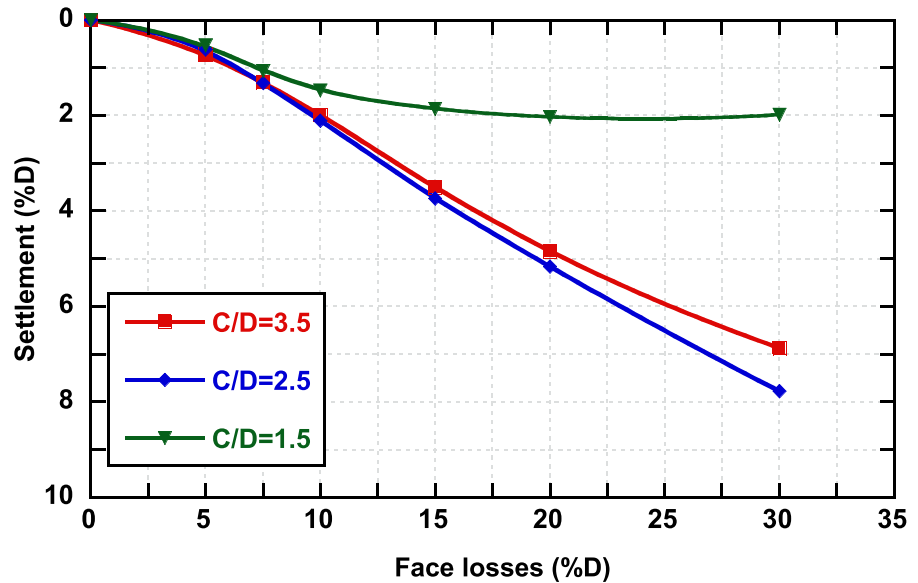
between volume and face loss. However, the embedded plane was positioned close to the tunnel face and is thus expected to be at or near the area of maximum settlement. Thus, the effect on the relationship is expected to be small especially in the context of small-scale modelling.

4.3.1 Analysis of Surface Settlements

The relationship between the face losses and the surface settlement at various *C/D* ratios is shown in Fig. 11. For C/D = 1.5, surface settlement increases rapidly till face loss reaches 15%D, where settlement reaches its peak and remained constant after that. For C/D = 2.5 and 3.5, surface settlement increases with face movement throughout the experiment. Shiau and Sams (2017) also observed a trend of increasing maximum settlement in clay at the point of collapse at a C/D = 2, which is consistent with the observations reported herein.

Surface settlement is compared for various *C/D* ratios at fixed face losses is presented in Fig. 12. The

Fig. 10 Volume loss due to face losses at different cover-to-diameter ratios
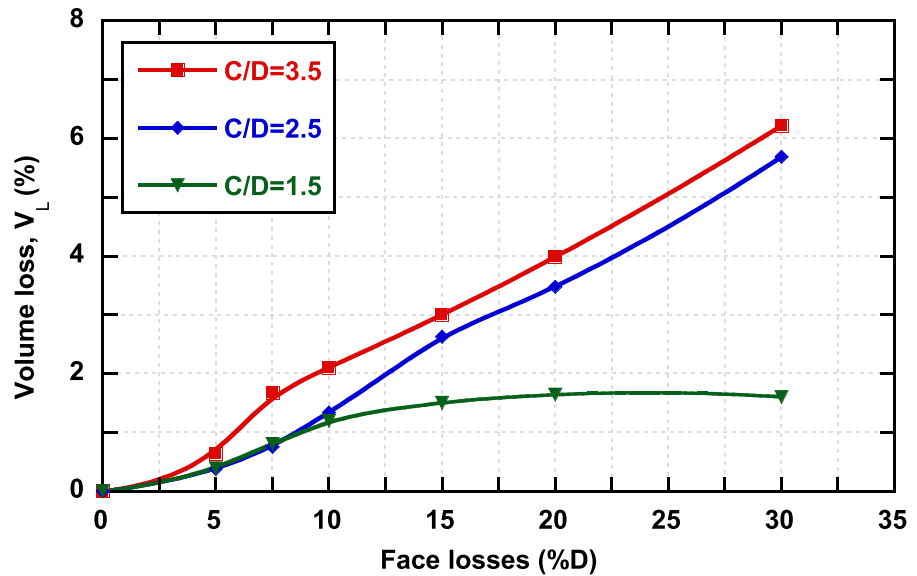
maximum surface settlement for C/D = 1.5 is significantly higher than it is for C/D = 2.5 and 3.5 at face loss 5%D. This behavior is consistent till face loss reaches 15%D, where settlement for C/D = 1.5 reaches its peak. Below face loss of 15%D, there is not much difference between surface settlement at cover-to-diameter ratio C/D = 2.5 and C/D = 3.5. With further increase in *C/D* we may see no effect on the surface settlement. However, when *C/D* ratio reduces from 2.5 to 1.5, the surface settlement drastically increases.

Surface vertical settlement decreases with the increase in *C/D* ratios which is evident from the settlement data presented in Fig. 12. At face loss 5%D and C/D = 1.5, surface settlement was approximately twice than that for C/D = 2.5 and 3.5, at the same face loss. Mair et al. (1993) presented similar findings in their research.

Asymmetry of surface and subsurface settlement is observed in the measurements presented in both Figs. 11 and 12, respectively. The asymmetry increases with the increase of the C/D ratio as well as with the increase of face losses. This may be due to undocumented variations in the undrained shear strength within the model. The effect appears to be small near the surface where the strength is lowest, with little to no effect for C/D = 1.5. However, with

the increase in C/D and the soil strain as face losses exceed 15%D asymmetry becomes larger.

4.3.2 Analysis of Sub-Surface Settlements

Vu et al. (2015) concluded that, a cover-to-diameter ratio *C/D* in the range of 0.5–1 is the shallowest practical ratio for tunneling since the design depth of the tunnel must accommodate the existence of utilities and other infrastructure systems. The observed subsurface settlements are presented at a plane located 1D above the tunnel crown for *C/D* of 2.5 and 3.5 in Fig. 13. The observed plane is thus located 0.5 D and 1.5D below the surface of the transparent clay surrogate for C/D = 2.5 and 3.5 respectively. The maximum subsurface settlements at the observed plane for C/D = 2.5 and 3.5 for different face losses are shown in Fig. 14. It is evident from Fig. 13 that subsurface settlements increase with the increase in face losses. However, subsurface settlement decreases with the increase in *C/D* ratio when measured at the same plane from tunnel crown level. In addition, rate of subsurface settlement increment increases with the increase in face losses (Fig. 14).
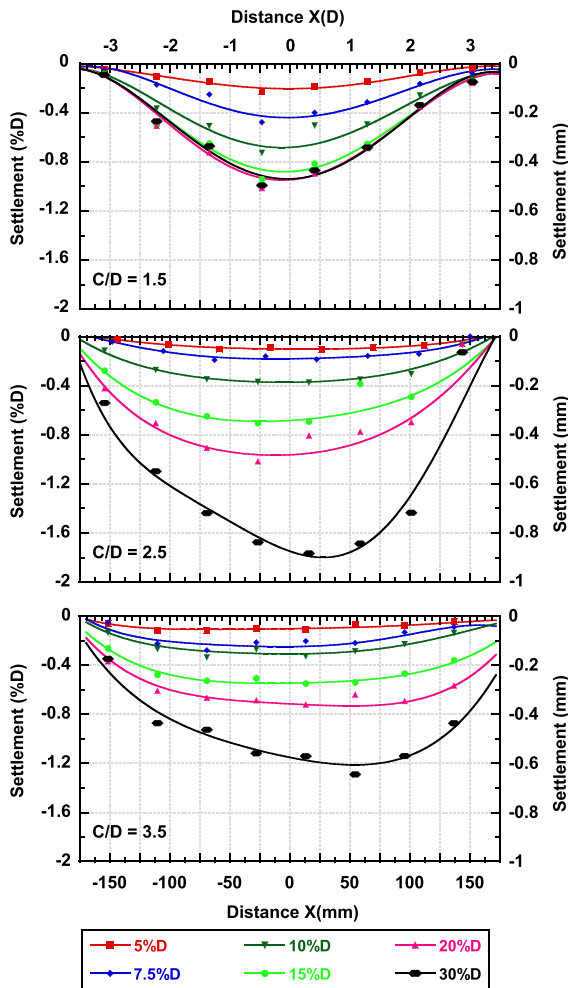
Fig. 11 Surface settlement due to change in face losses at fixed cover-to-diameter ratio

4.4 Comparison of Measured and Theoretical Settlements

The relationship between the theoretical surface and subsurface settlement and measured values is explored. Theoretical subsurface settlements were computed using Eqs. (1)–(3) and compared to experimentally determined values shown in Fig. 13. Comparison is presented at several observation planes located at a depth of 0.75D below the surface of the transparent clay surrogate, as well as at the transparent clay surrogate surface for C/D = 2.5 (Fig. 15). For

C/D = 3.5 a third observation plane located 1.5D above the tunnel crown is also added (Fig. 16). The magnitude of surface settlements along the centerline is generally consistent with the theoretical values, although the shape deviates somewhat from the Gaussian assumption. For C/D = 2.5, the experimental and theoretical maximum subsurface settlements are consistent. However, the shape of the settlement trough deviates from the Gaussian assumption. A more pronounced deviation from the theoretical predictions can be observed in C/D = 3.5 in terms of magnitude as well as shape. This is believed to have resulted from the low shear strength of the surrogate clay. It is noteworthy that the Gaussian curve has been developed largely using stronger soils. So, the deviation may represent behavior to be expected in soft marine clays.

5 Limitations

The use of a transparent surrogate to model the behavior of natural soils offers many advantages in visualizing the internal response of the soil continuum. At the same time the technique introduces a number of limitations, as follows:

- The size of the physical model was limited to prevent transparency degradation. The tunnel was located 3.5D from the boundaries to reduce boundary effects. Nevertheless, model boundaries may have contributed to some edge effects.
- The effect of gravity is not scaled appropriately due to the 1 g nature of the model; however, the strength of clays is generally less dependent on scaling the gravitational field than sands. Therefore, failure to scale the effect of gravity is believed to be small.
- The use of a trap door to model ground response in the tunnel crown does not simulate the actual tunneling process as various shield operation parameters cannot be taken into account; thus only approximate estimate of the surface and subsurface settlement can be obtained. In addition, the observed deformations are less reliable at the tunnel/soil interface.
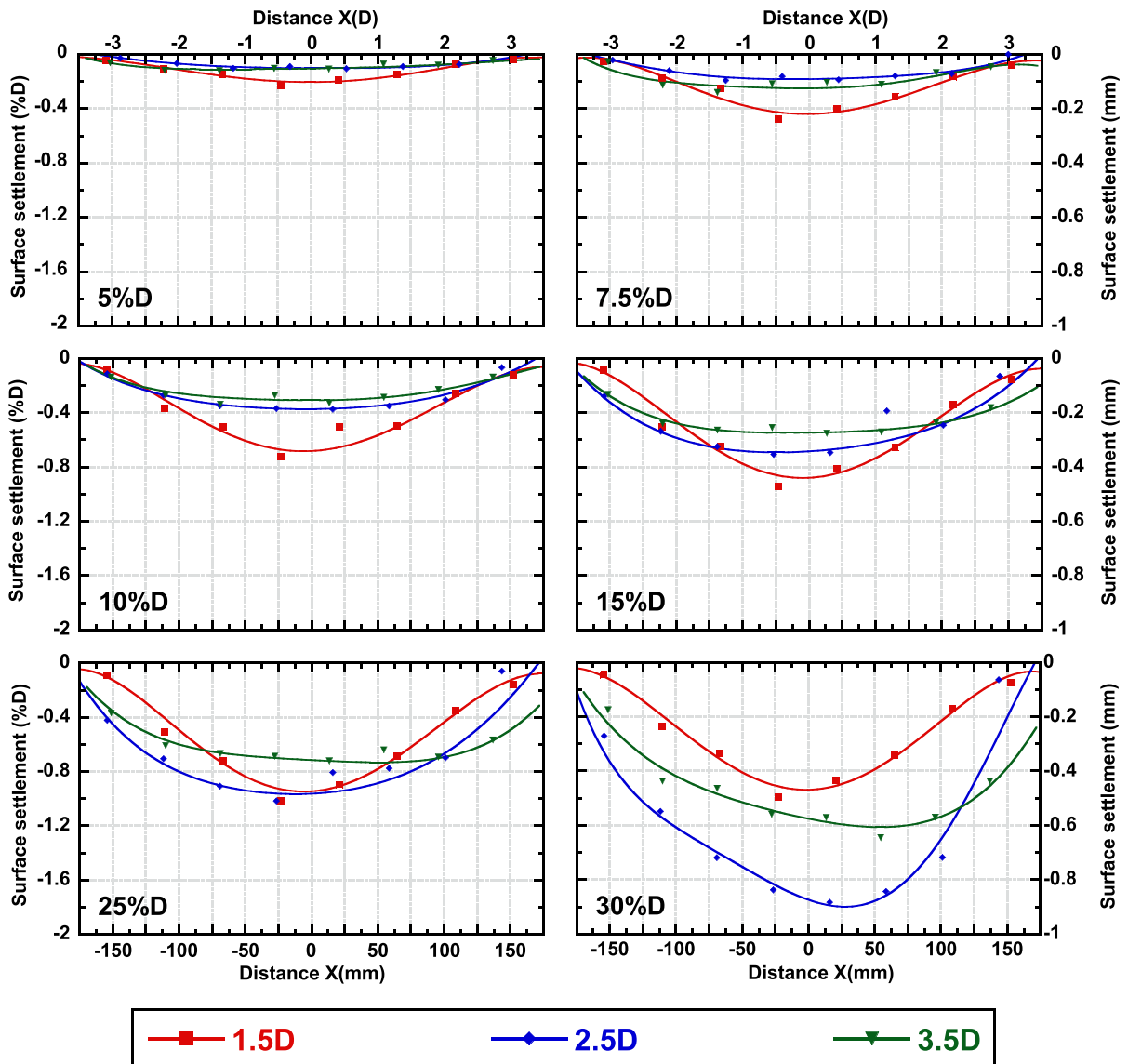
Fig. 12 Surface settlement due to change in cover-to-diameter ratio at fixed face losses

- The effect of cover-to-diameter (*C/D*) ratio on settlement often depends on the lateral earth pressure coefficient, elastic modulus of soil and lining materials, stress history and hardening of lining materials if shotcrete or any other cast-in-place cementitious materials is used. These parameters were not considered in this simplified tunneling induced settlement visualization using trapdoor models as discussed by Meguid et al. (2008).

- Although the layered system employed in this model study is representative of some urban stratigraphies consisting of soft marine soil underlaying urban fill or alluvial sands, the findings should be applied with caution. In particular, the relative strength, thickness, and unit weight should be considered when results are applied to different stratigraphies. It is noteworthy that, all surface settlement values were considered at the surface of the clay layer due to the inability to collect the

Fig. 13 Subsurface settlement due to change in face losses at a fixed plane located 1.0D from the tunnel crown for cover-to-diameter ratio 2.5 and 3.5

6 Conclusions
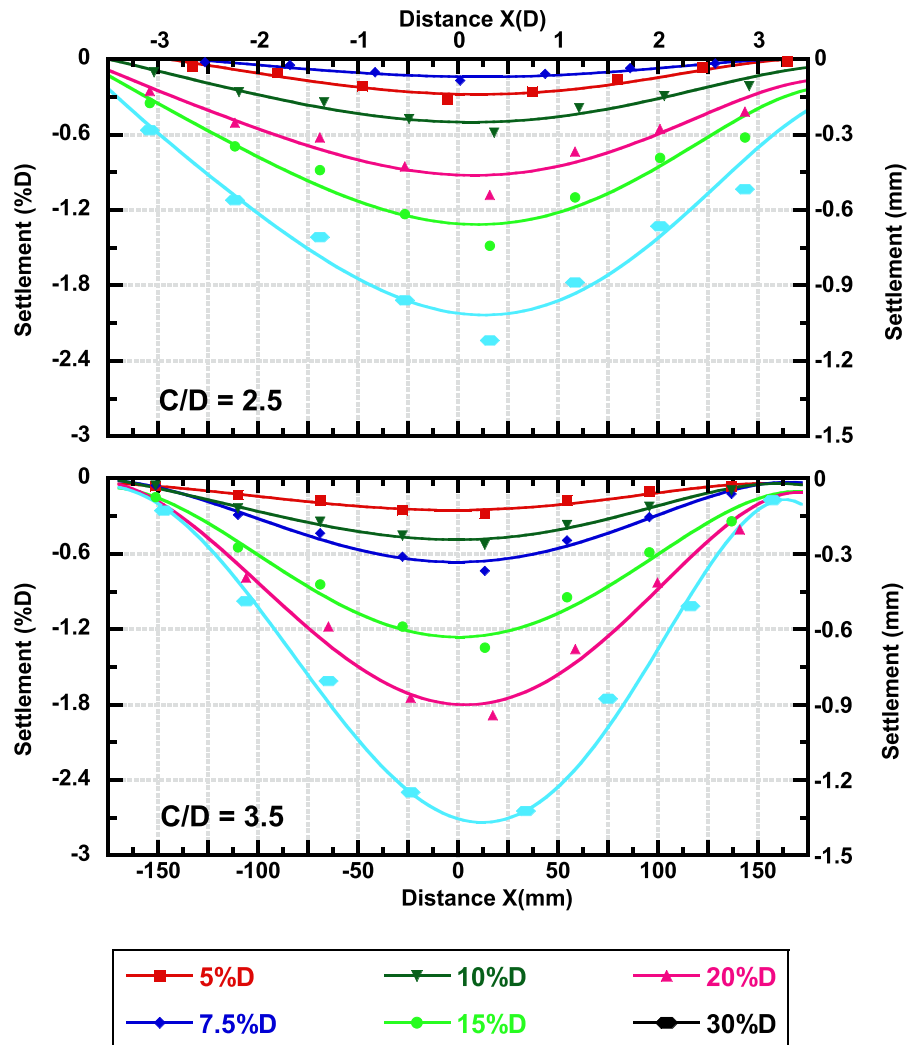
This study demonstrates that the cover-to-diameter (*C/ D*) ratio significantly affects both surface and subsurface settlements occurring during tunneling in soft clay. *C/D* ratio also affects arching actions and contributes to tunnel stability. Spatial soil required information within the opaque sand layer, which was treated in this study as a surcharge load.

deformations due to increasing face losses were visualized with the aid of a transparent soil representing the behavior of soft clay. The following observations represent a brief summary of the findings from this study:

- Both surface and subsurface settlement increases with the increase in face losses. Surface settlement decreases with the increase in *C/D* ratio, while subsurface settlements increase with increasing *C/ D* ratio.

Fig. 14 Maximum subsurface settlement at a fixed plane located 1.5D above the tunnel crown
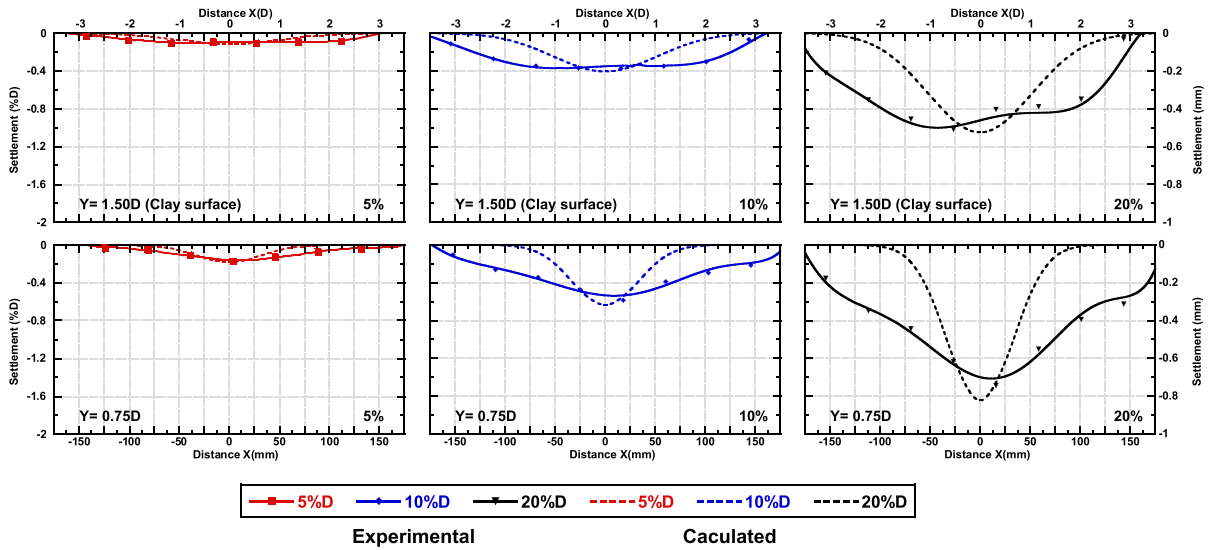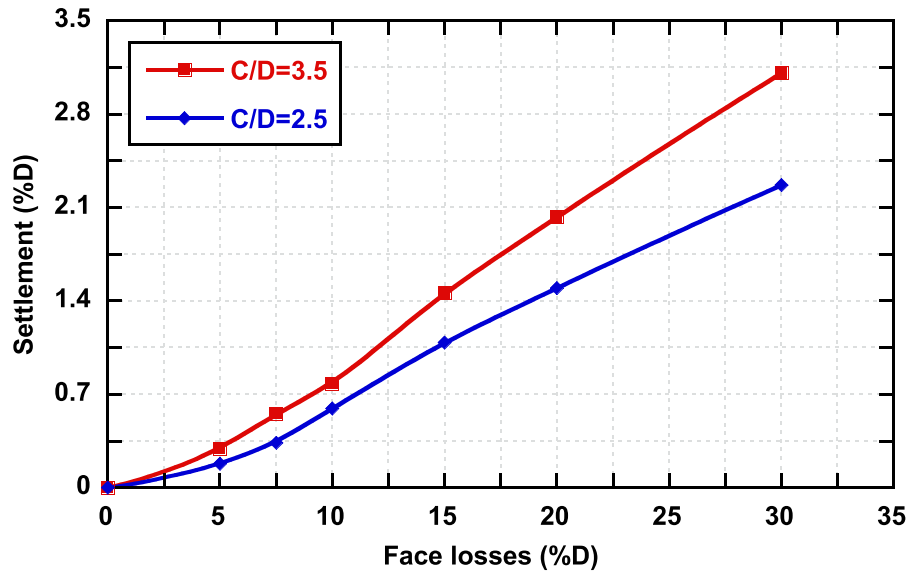

Fig. 15 Comparison between the experimental and calculated settlements for tunnel with C/D = 2.5 at face losses of 5%D, 10%D and 20%D (Settlements shown at 2 elevations, where Y is the vertical distance measured from the tunnel crown)

- Subsurface settlements are significantly larger than surface settlements, which may adversely affect the behavior of subsurface foundations and utilities.
- Settlement troughs were generally wider in this study than the values predicted using conventional Gaussian distributions, presumably due to the weak shear strength of the soil surrogate. Therefore, it is believed that while the conventional Gaussian distribution is reasonable for most soils,

it may under predict the zone of influence in soft clays.
- Significant arching effects were observed to occur at a cover-to-diameter ratio of C/D = 1.5 and 2.5. For C/D = 3.5, the arching affects slowly disappears and the soil further spread out around the tunnel crown with each increment of face loss. This finally resulted in establishing a wider settlement trough. Observed arching action also affects
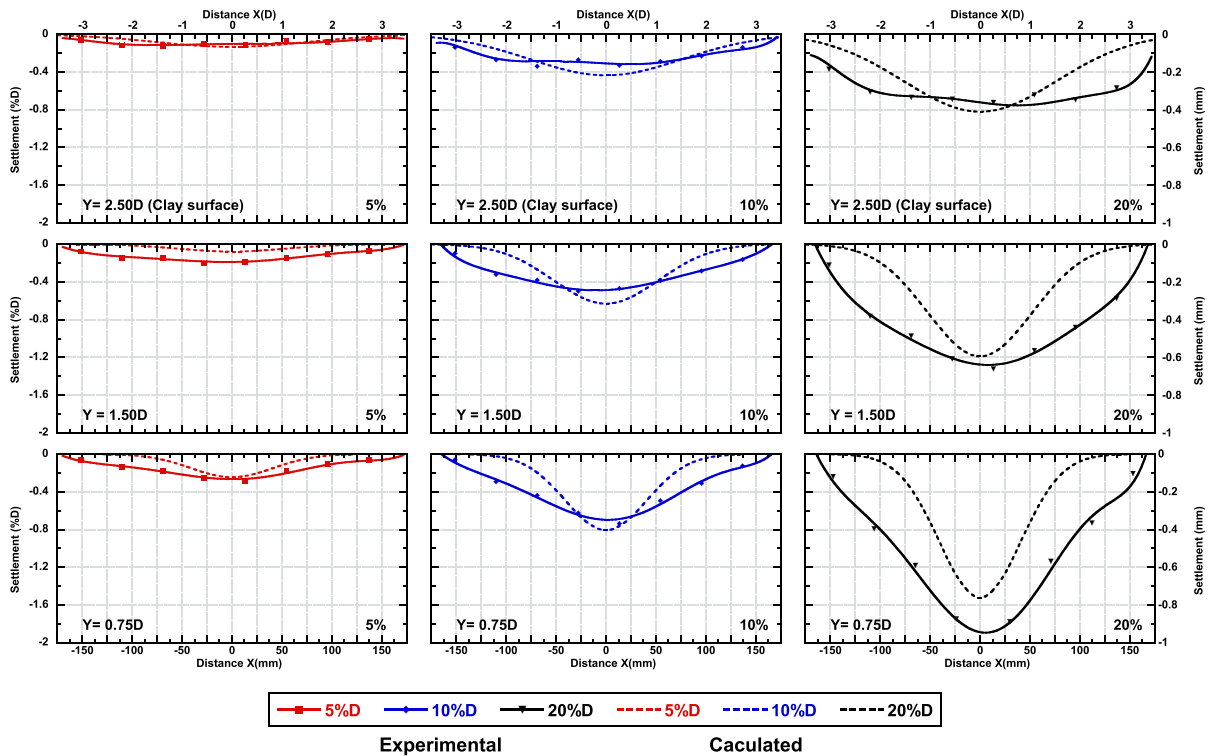
Fig. 16 Comparison between the experimental and calculated settlements for tunnel with C/D = 3.5 at face losses of 5%D, 10%D and 20%D (Settlements shown at 3 elevation levels and Y is the vertical distance measured from the tunnel crown)

collapse and dissipating arching action may therefore impact tunnel crown stability.

- With the increase in face losses, the shear strain increases, and a distinct shear failure is observed for *C/D* ratio of 2.5 and 3.5, but not for *C/D* = 1.5. The shear plane was tangent to a circle circumscribing the tunnel but located 1–2 D outside of the tunnel making a 45° angle with the horizontal surface.

- For C/D = 1.5, soils around the tunnel were only subject to dilation. With the increase of *C/D* ratio, compression starts at face losses of 15%D and increases with the increase in face losses. The compression area extends in small segregated pockets that reach the surface.

Declarations

Conflicts of interest The authors declare that they have no conflict of interest.

References

Adachi T, Kimura M, Nishimura T, Koya N (1997) Trap door experiment under centrifugal conditions. Deform Progress Fail Geomech, 725–730

Ads A, Iskander M, Bless S (2020a) Soil–projectile interaction during penetration of a transparent clay simulant. Acta Geotech 15:815–826. https://doi.org/10.1007/s11440-020-00921-z

Ads A, Iskander M, Bless S (2020b) Shear strength of a synthetic transparent soft clay using a miniature ball penetrometer test. Geotech Test J. https://doi.org/10.1520/GTJ20190020

Ahmed M, Iskander M (2011) Analysis of Tunneling-Induced Ground Movements Using Transparent Soil Models. J Geotech Geoenvironmental Eng 137:525–535. https://doi.org/10.1061/(asce)gt.1943-5606.0000456

Ahmed M, Iskander M (2012) Evaluation of tunnel face stability by transparent soil models. Tunn Undergr Sp Technol 27:101–110. https://doi.org/10.1016/j.tust.2011.08.001

Arshad MI, Tehrani FS, Prezzi M, Salgado R (2014) Experimental study of cone penetration in silica sand using digital image correlation. Géotechnique 64:551–569

Atkinson JH, Potts DM (1977) Stability of a shallow circular tunnel in cohesionless soil. Géotechnique 27:203–215. https://doi.org/10.1680/geot.1977.27.2.203

Atkinson JH, Orr TLL, Potts DM (1975) Research studies into the behaviour of tunnels and tunnel linings in soft ground

Attewell P (1978) Ground movements caused by tunnelling in soil

Attewell PB, Yeates J, Selby AR (1986) Soil movements induced by tunnelling and their effects on pipelines and structures

Beemer RD, Aubeny CP (2012) Digital image processing of drag embedment anchors in translucent silicate gel. In: Proceedings on GeoManitoba

Beemer RD, Shaughnessy E, Ewert KR et al (2016) The use of sodium pyrophosphate to improve a translucent clay simulate. In: Geo-Chicago 2016. pp 83–93. https://doi.org/10.1061/9780784480151.009

Chambon P, Corté JF (1994) Shallow tunnels in cohesionless soil: Stability of tunnel face. J Geotech Eng 120:1148–1165. https://doi.org/10.1061/(ASCE)0733-9410(1994)120:7(1148)

Chen Z, Omidvar M, Iskander M (2016) Observations of multi-scale granular kinematics around driven piles in plane strain condition. Geotech Test J 39:827–841. https://doi.org/10.1520/GTJ20150199

Chen Z, Omidvar M, Iskander M, Bless S (2015) Visualizing the fundamental physics of rapid earth penetration using transparent soils. Geotech Spec Publ GSP 256:2617–2626. https://doi.org/10.1061/9780784479087.243

Chini CM, Wallace JF, Rutherford CJ, Peschel JM (2015) Shearing failure visualization via particle tracking in soft clay using a transparent soil. Geotech Test J 38:708–724. https://doi.org/10.1520/GTJ20140210

Clough GW, Schmidt B (1981) Design and performance of excavations and tunnels in soft clay. Elsevier Scientific Publishing Company, Amsterdam

Cording EJ (1991) Control of ground movements around tunnels in soil. In: Ninth Pan American Conference, Vina del Mar, Chile. Sociedad Chilena de Geotechina, pp 2195–2244

Cording EJ (1975) Displacement around soft ground tunnels, General Report: Session IV, Tunnels in soil. In: Proceedings of 5th Panamerican Congress on SMFE

Cording EJ, O'Rourke TD, Boscardin M (1978) Ground movements and damage to structures. In: Evaluation and prediction of subsidence. ASCE, pp 516–537

Davis EH, Gunn MJ, Mair RJ, Seneviratne HN (1980) The stability of shallow tunnels and underground openings in cohesive material. Geotechnique 30:397–416. https://doi.org/10.1680/geot.1980.30.4.397

Dimmock PS, Mair RJ (2007) Volume loss experienced on open-face London Clay tunnels. Proc Inst Civ Eng Geotech Eng 160:3–11. https://doi.org/10.1680/geng.2007.160.1.3

Dyer MR, Hutchinson MT, Evans N (1996) Sudden Valley Sewer: a case history. In: Geotechnical aspects of underground construction in soft ground, pp 671–676

Ezzein FM, Bathurst RJ (2011) A transparent sand for geotechnical laboratory modeling. Geotech Test J 34:1–12. https://doi.org/10.1520/GTJ103808

Gnilsen R (1989) Numerical analysis, underground structures design and instrumentation

Hird CC, Stanier SA (2010) Modelling helical screw piles in clay using a transparent soil. Phys Model Geotech - Proc 7th Int Conf Phys Model Geotech 2010 ICPMG 2010 2:769–774. https://doi.org/10.1201/b10554-126

Idinger G, Aklik P, Wu W, Borja RI (2011) Centrifuge model test on the face stability of shallow tunnel. Acta Geotech 6:105–117. https://doi.org/10.1007/s11440-011-0139-2

Iskander M (2010) Modelling with transparent soils: visualizing soil structure interaction and multi phase flow, non-intrusively. Springer, Berlin

Iskander M, Bless S, Omidvar M (2015) Rapid penetration into granular media: visualizing the fundamental physics of rapid earth penetration. Elsevier, Amsterdam

Iskander MG, Liu J, Sadek S (2002) Transparent Amorphous Silica to Model Clay. J Geotech Geoenvironmental Eng 128:262–273. https://doi.org/10.1061/(asce)1090-0241(2002)128:3(262)

Karakus M, Fowell RJ (2003) Effects of different tunnel face advance excavation on the settlement by FEM. Tunn Undergr Sp Technol 18:513–523. https://doi.org/10.1016/S0886-7798(03)00068-3

Kirsch A (2010) Experimental investigation of the face stability of shallow tunnels in sand. Acta Geotech 5:43–62. https://doi.org/10.1007/s11440-010-0110-7

Kong XX, Liu QS, Zhang QB et al (2018) A method to estimate the pressure arch formation above underground excavation in rock mass. Tunn Undergr Sp Technol 71:382–390. https://doi.org/10.1016/j.tust.2017.09.004

Lee Y, Yoo C (2006) Behaviour of a bored tunnel adjacent to a line of loaded piles. Tunn Undergr Sp Technol 21:370. https://doi.org/10.1016/j.tust.2005.12.185

Lee YJ, Bassett RH (2007) Influence zones for 2D pile-soil-tunnelling interaction based on model test and numerical analysis. Tunn Undergr Sp Technol 22:325–342. https://doi.org/10.1016/j.tust.2006.07.001

Lee CJ, Wu BR, Chen HT, Chiang KH (2006) Tunnel stability and arching effects during tunneling in soft clayey soil. Tunn Undergr Sp Technol 21:119–132. https://doi.org/10.1016/j.tust.2005.06.003

Liu J, Iskander M (2004) Adaptive cross correlation for imaging displacements in soils. J Comput Civ Eng 18:46–57. https://doi.org/10.1061/(ASCE)0887-3801(2004)18:1(46)

Liu J, Iskander MG (2010) Modelling capacity of transparent soil. Can Geotech J 47:451–460. https://doi.org/10.1139/t09-116

Loganathan N, Poulos HG (1998) Analytical prediction for tunneling-induced ground movements in clays. J Geotech Geoenvironmental Eng 124:846–856. https://doi.org/10.1061/(ASCE)1090-0241(1998)124:9(846)

Mair RJ, Taylor RN (1997) Theme lecture: Bored tunnelling in the urban environment. In: Proceedings of the fourteenth international conference on soil mechanics and foundation engineering. Rotterdam, pp 2353–2385

Mair RJ, Taylor RN, Bracegirdle A (1993) Subsurface settlement profiles above tunnels in clays. Geotechnique 43:315–320. https://doi.org/10.1680/geot.1995.45.2.361

Marshall AM, Farrell R, Klar A, Mair R (2012) Tunnels in sands: The effect of size, depth and volume loss on greenfield displacements. Geotechnique 62:385–399. https://doi.org/10.1680/geot.10.P.047

Mašín D (2009) 3D Modeling of an NATM Tunnel in High K0 Clay Using Two Different Constitutive Models. J Geotech Geoenvironmental Eng 135:1326–1335. https://doi.org/10.1061/(asce)gt.1943-5606.0000017

Meguid MA, Saada O, Nunes MA, Mattar J (2008) Physical modeling of tunnels in soft ground: A review. Tunn Undergr Sp Technol 23:185–198. https://doi.org/10.1016/j.tust.2007.02.003

Mesri G, Ajlouni M (2007) Engineering properties of fibrous peats. J Geotech Geoenviron Eng 133:850–866. https://doi.org/10.1061/(asce)1090-0241(2007)133:7(850)

Moh ZC, Ju DH, Hwang RN (1996) Ground movements around tunnels in soft ground. In: Proceedings of symposium on geotechnical aspects of underground construction in soft ground, pp 725–730

Ni Q, Hird CC, Guymer I (2010) Physical modelling of pile penetration in clay using transparent soil and particle image velocimetry. Geotechnique 60:121–132. https://doi.org/10.1680/geot.8.P.052

O'Reilly MP, New BM (1982) Settlements above tunnels in the United Kingdom—their magnitude and prediction

Omidvar M, Chen Z, Iskander M, (2015) Image-based Lagrangian analysis of granular kinematics. J Comput Civ Eng 29:04014101. https://doi.org/10.1061/(asce)cp.1943-5487.0000433

Omidvar M, Iskander M, Bless S (2016) Soil–projectile interactions during low velocity penetration. Int J Impact Eng 93:211–221. https://doi.org/10.1016/j.ijimpeng.2016.02.015

Oñate E (2013) Structural analysis with the finite element method. Linear statics: volume 2: beams, plates and shells. Springer, Berlin

Park KH (2005) Analytical solution for tunnelling-induced ground movement in clays. Tunn Undergr Sp Technol 20:249–261. https://doi.org/10.1016/j.tust.2004.08.009

Park SH, Adachi T (2002) Laboratory model tests and FE analyses on tunneling in the unconsolidated ground with inclined layers. Tunn Undergr Sp Technol 17:181–193. https://doi.org/10.1016/S0886-7798(02)00003-2

Peck RB (1969) Deep excavations and tunneling in soft ground. In: Proceedings on 7th ICSMFE, pp 225–290

Rowe RK, Lee KM (1992) Subsidence owing to tunnelling. II. Evaluation of a prediction technique. Can Geotech J 29:941–954

Sadek S, Iskander MG, Liu J (2003) Accuracy of digital image correlation for measuring deformations in transparent media. J Comput Civ Eng 17:88–96. https://doi.org/10.1061/(ASCE)0887-3801(2003)17:2(88)

Schofield AN (1980) Cambridge Geotechnical Centrifuge Operations. Geotechnique 30:227–268. https://doi.org/10.1680/geot.1980.30.3.227

Shiau J, Sams M (2017) Estimation of tunneling induced ground settlement using pressure relaxation method. Int J GEOMATE 13:132–139. https://doi.org/10.21660/2017.39.85076

Skempton AW (1957) Discussion of "The planning and design of the new Hong Kong Air Port". In: Proceedings on Institute of Civil Engineering, pp 305–307

Sun J, Liu J (2014) Visualization of tunnelling-induced ground movement in transparent sand. Tunn Undergr Sp Technol 40:236–240. https://doi.org/10.1016/j.tust.2013.10.009

Terzaghi K, Peck RB, Mesri G (1996) Soil mechanics in engineering practice. Wiley, Hoboken

Thongprapha T, Fuenkajorn K, Daemen JJK (2015) Study of surface subsidence above an underground opening using a trap door apparatus. Tunn Undergr Sp Technol 46:94–103. https://doi.org/10.1016/j.tust.2014.11.007

Vu MN, Broere W, Bosch J (2015) The impact of shallow cover on stability when tunnelling in soft soils. Tunn Undergr Sp Technol 50:507–515. https://doi.org/10.1016/j.tust.2015.09.005

Vu MN, Broere W, Bosch J (2016) Volume loss in shallow tunnelling. Tunn Undergr Space Technol 59:77–90. https://doi.org/10.1016/j.tust.2016.06.011

Wallace JF, Rutherford CJ (2015) Geotechnical properties of LAPONITE RD®. Geotech Test J 38:574–587. https://doi.org/10.1520/GTJ20140211

Welker AL, Bowders JJ, Gilbert RB (1999) Applied Research Using a Transparent Material with Hydraulic Properties Similar to Soil. Geotech Test J 22:266–270. https://doi.org/10.1520/gtj11117j

Welker AL, Gilbert RB, Bowders JJ (2000) Using a reduced equivalent diameter for a prefabricated vertical drain to account for smear. Geosynth Int 7:47–57

Zhang ZX, Liu C, Huang X (2017) Numerical analysis of volume loss caused by tunnel face instability in soft soils. Environ Earth Sci 76:1–19. https://doi.org/10.1007/s12665-017-6893-1